Article

Dual-Beam Steerable TMAs Combining AM and PM Switched Time-Modulation

Roberto Maneiro-Catoira [ID], Julio Brégains [ID], José A. García-Naya *[ID] and Luis Castedo [ID]

CITIC Research Center, Department of Computer Engineering, University of A Coruña, Campus de Elviña, 15071 A Coruña, Spain; roberto.maneiro@udc.es (R.M.-C.); julio.bregains@udc.es (J.B.); luis@udc.es (L.C.)
* Correspondence: jagarcia@udc.es

Abstract: Wireless sensor networks (WSN) are increasingly requiring directional antennas that not only provide higher capacity, security, transmission range or robustness against interference, but also contribute with smart antenna capabilities such as adaptive beamforming or multi beam radiation patterns. Standard phased arrays provide these features, but employing feeding networks based on digitally controlled variable phase shifters (VPSs) which have the disadvantage of high cost and limited angular resolution. Instead, time-modulated arrays (TMAs) use switched feeding networks governed by digital periodic sequences which allow harmonic patterns to be radiated and endows (TMAs) with attractive multifunctional capabilities. In this paper, we analyze and properly combine (TMA) switched feeding networks capable of time-modulating an antenna array with discretized amplitude modulation (AM) and phase modulation (PM) waveforms. The advantages of the proposed innovative dual-beam (TMA) with respect to the competing architectures are, on the one hand, its power efficiency and beamsteering (BS) phase sensitivity and, on the other, its hardware simplicity, which allows for an excellent relative cost advantage.

Keywords: time-modulated arrays; wireless sensor networks; beam steering; multibeam

1. Introduction

A wireless sensor network (WSN) often consists of spatially distributed autonomous sensors nodes—capable of monitoring in real-time certain physical variables—and one or more base stations connected to the end-users [1]. Major handicaps of WSNs, which typically use omnidirectional antennas, are their need for low energy consumption and a restricted cost of the nodes as well as the guarantee of secure wireless communications within the network.

Contrarily to omnidirectional antennas, directional antennas focus the transmitted power in a narrow radiation region, thus reducing the energy usage and the risk of jammers/eavesdroppers attacks. In addition, by enabling longer transmission distances, they facilitate the use of fewer hops and reduce the risk of any node to become isolated [2]. Hence, the use of directional antennas in WSN allows for improved power and security constraints, but at the expense of a higher complexity [3]. Furthermore, if the nodes are endowed with smart-antenna extra functionalities such as beam steering, direction finding, secure signal transmissions, etc., the antenna feeding network will need to be equipped with variable phase shifters (VPSs), which will substantially increase the costs and radiation power losses. In this regard, the benefits of using directional antennas built with switched beamforming networks (BFNs) rather than VPSs have been investigated [4,5] but in these approaches the utility of the switches consists in shifting between a set of possible positions for different radiation patterns.

A time-modulated array (TMA) is a type of adaptive antenna array which employs switches in the antenna BFN but in a completely different way [6]. The radiation pattern of a TMA is controlled by applying periodical pulses (with fundamental period T_0) to

the individual array elements by means of radio frequency (RF) switches. Such a time-modulation causes the TMA to generate radiation patterns at frequencies $\omega_c \pm q\omega_0$, where $q \in \mathbb{N}$, ω_c is the carrier frequency, and $\omega_0 = 2\pi/T_0$ represents the time-modulation frequency [6]. The attractiveness of using TMAs in WSNs lies mainly in three aspects:

1.   The low cost and insertion losses of the array feeding network.
2.   The easy and precise method for realising electronic beamsteering by simply controlling the on-off switching instants [7].
3.   The utilization of a single RF chain which results in significant savings in power consumption in applications such as simultaneous multi-node communication [8] or channel diversity extraction in multipath wireless reception [9].
4.   The ability to transform spatial diversity into frequency diversity which enable smart antenna extra functionalities like direction of arrival (DOA) estimation [10–12] or secure communications [13,14], among others.

Despite these advantages, and contrarily to the case of standard phased arrays, the design of TMAs involves dealing with issues that affect the antenna efficiency, namely

1.   The difficulty of removing (or strongly attenuate) the unexploited harmonics, including the harmful frequency-mirrored beam patterns. In this sense, the design of the so-called single sideband (SSB) TMAs is of great significance [7,15,16].
2.   The presence of signal losses caused by the particular hardware architecture of the TMA switching network [17,18].

Although the design of SSB multibeam TMAs has already been addressed in the literature [18], the corresponding approaches are based on switched BFNs in which amplitude modulation (AM) is exclusively employed. Hence, phase modulation (PM) is not considered. In this work, a fair comparison is made between the two modulation methods when applied to TMAs. Despite that, when considering the same number of discretization levels, AM BFNs allow for a better rejection of unwanted harmonics than PM ones, and the former have the disadvantage of an increased complexity due to the use of power splitters/combiners.

The main contribution of this paper is the design of efficient dual-beam SSB TMAs based on the combination of switched networks, which are simpler than those in [18], capable of generating discretized AM and PM periodic time-modulating signals, and being well-suited for WSN application.

The remainder of the paper is structured as follows. In Section 2, after individually analyzing the spectral characteristics of continuous sinusoidal AM waveforms and continuous linear-phase PM waveforms, we consider the implementation of discretized versions of such signals by means of switched architectures. In Section 3, we combine the previous AM and PM feeding networks to characterize dual-beam steerable TMAs. Section 4 contains numerical simulation results and their discussion. Section 5 compares the proposed dual-beam SSB TMAs with existing dual-beam architectures. Finally, Section 6 is devoted to the conclusions.

2. AM and Linear-Phase PM Modulation with Switched Networks

In this section, we start analyzing the original target modulating signals in the analog domain and then we present their corresponding discretized implementations. We study also their characteristics and their implementation with switches.

2.1. AM and PM Periodic Modulating Signals

We will begin by interpreting Figure 1 from a TMA perspective. Let us take the simplest case: if we time-modulate each of the the static excitations of a uniform linear array (ULA) with the same periodic signal $p(t)$ with fundamental period T_0, the radiation patterns appear at frequencies $\omega_c \pm q\omega_0$ and the q-th order Fourier coefficient of $p(t)$ will become the excitation of each element in the corresponding array factor (AF) at the frequency $\omega_c + q\omega_0$. Hence, intuitively, if we only vary the modulus of the Fourier coefficients (by

varying the periodic signals applied to each element), we can modify the topology of the q-th power radiated pattern and if we only modify the phases of the coefficients we can shift (i.e., steer) such a power radiated pattern.

When time modulating a ULA with a pure sinusoidal signal (Figure 1a), only two harmonic patterns are generated at the frequencies $\omega_c \pm \omega_0$ (Figure 1c). The fact that the frequency $\omega_c + \omega_0$ appears with its mirrored counterpart $\omega_c - \omega_0$ means that we have a double sideband (DSB) TMA, which generates harmonic diagrams with the same shape (Fourier coefficients with the same modulus), but pointing towards directions that are symmetric (opposite phase) with respect to the broadside of the array. In other words, both harmonics do not have independent phases and it is not possible to steer them independently, thus loosing flexibility and energy efficiency. Hence, although in this work we will profitably exploit the DSB feature of discretized sinusoids to perform independent dual-beamsteering (as we will see in the ensuing section), TMA research generally focuses on the synthesis of SSB TMAs without frequency-mirrored beampatterns.

In this sense, if we consider the periodic extension of a linear-phase PM waveform (Figure 1b), we observe that it has a single nonzero Fourier coefficient at $q = 1$ (see Figure 1d). Therefore, if we apply such a periodic pulse to time-modulate the elements of a ULA, we will obtain a single harmonic pattern at $\omega_c + \omega_0$, thus achieving SSB TMA capabilities.
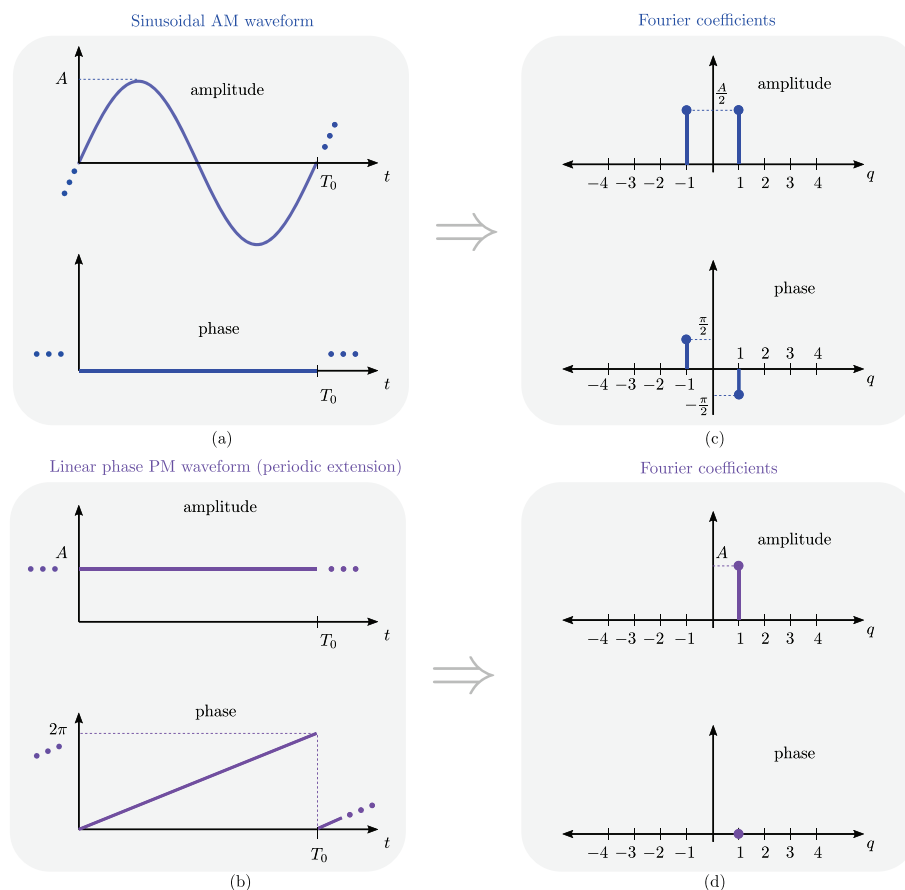

Figure 1. Representation of amplitude and phase versus time. (**a**) A sinusoidal AM waveform with period T_0. (**b**) The periodic extension of a linear-phase PM waveform. (**c**,**d**) The Fourier coefficients versus q of the corresponding signals in (**a**,**b**), respectively (notice that the q-th coefficient accounts for the spectral component at the frequency $q2\pi/T_0$).

Finally, notice that if P_q are the Fourier coefficients of a periodic signal $p(t)$, then $e^{-j\omega_0 q\tau}P_q$ are the Fourier coefficients of $p(t - \tau)$. Consequently, if $p(t)$ (which could represent the signal in Figure 1a or in Figure 1b) is time-shifted, then the phases of its Fourier

coefficients are modified proportionally to the time delay τ and, accordingly, the q-th harmonic pattern can be steered to a given direction.

2.2. Discretization of the Modulating Signals: Characteristics and Generation

In this work, we will consider two types of waveform discretization. One is shown in Figure 2 and uses only four different levels. Such a discretization has the particularity of being easily implementable by means of switch architectures. Figure 2a shows a four-level discretized version of a sinusoidal AM waveform denoted by $p^{\text{AM}}(t)$. We can observe in Figure 2c its normalized Fourier series power spectrum in dB, $20 \log_{10} \left| P_q^{\text{AM}} / P_1^{\text{AM}} \right|$, being P_q^{AM} the Fourier coefficient of order q. We can see, apart from the DSB character of the waveform, that $p^{\text{AM}}(t)$ is a very good approximation of the analog sine function because, although there are nonzero harmonics other than the useful ones ($q \pm 1$), they are all attenuated by at least 16.9 dB with respect to the useful harmonics. More specifically, $\Psi^{\text{AM}} = \{q = 2k + 1; k \in \mathbb{Z}\} = \{\dots, -5, -3, -1, 1, 3, 5, \dots\}$ is the set of indexes of the nonzero harmonics.
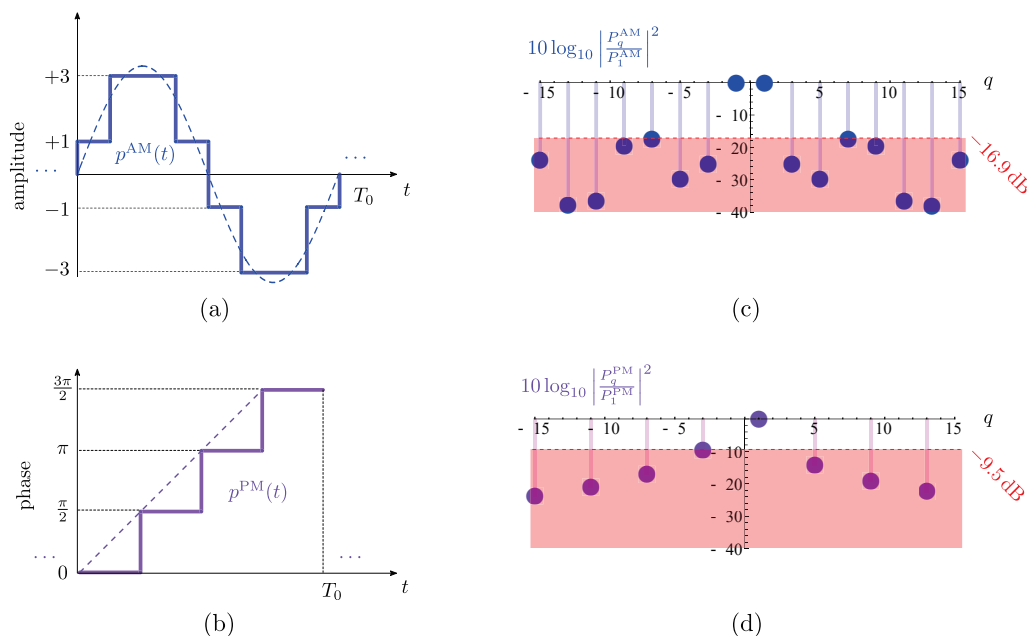

Figure 2. Four-level discretization of the waveforms shown in Figure 1: (**a**) discretized sinusoidal AM waveform (one period); (**b**) Discretized linear-phase PM waveform (one period). Normalized Fourier series power spectrum of the discretized waveforms: (**c**) AM waveform in (**a**); (**d**) PM waveform in (**b**).

Figure 2b shows a 4-level discretization of the periodical extension of a linear-phase PM waveform denoted $p^{\text{PM}}(t)$ and Figure 2d shows its corresponding normalized Fourier series power spectrum. Observe the SSB characteristic of the waveform while the most meaningful undesirable harmonic is the one with order $q = -3$ whose relative level is -9.5 dB with respect to the useful harmonic $q = 1$. Note that for this level of discretization, only harmonics whose order q belongs to the set $\Psi^{\text{PM}} = \{q = 4\Gamma - 3; \Gamma \in \mathbb{Z}\} = \{\dots, -7, -3, 1, 5, 9, 13, \dots\}$ are generated. The rejection level of unwanted harmonics can be improved by considering eight discretization levels, see Figure 3. It can be seen that in this case a minimum rejection of unwanted harmonics of at least -16.9 dB is achieved, being $\Psi^{\text{PM}} = \{q = 8\Lambda - 23; \Lambda \in \mathbb{Z}\} = \{\dots, -15, -7, 1, 9, 17, 25, \dots\}$ the set of indexes of the non-zero harmonics. Ultimately, to obtain the same level of rejection of unwanted harmonics, it is necessary to discretize the PM signal with twice as many levels as the AM signal.
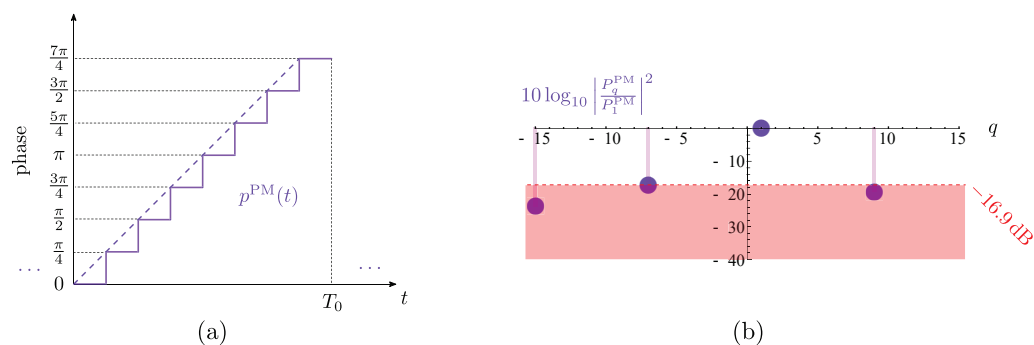
Figure 3. (**a**) Discretized linear-phase PM waveform (one period) with 8 levels. (**b**) Normalized Fourier series power spectrum of the discretized waveform.

Let us now focus on the design of the switching networks capable of implementing the discretized signals in Figure 2, starting with the discretized sinusoidal AM waveform $p^{\mathrm{AM}}(t)$ in Figure 2a. Such a waveform can be constructed as the sum of three periodic bipolar square pulses that have a certain fixed time delay between them [18]. Time modulating with $p^{\mathrm{AM}}(t)$ is efficiently implemented with the single-pole dual-throw (SPDT) switches connection shown in Figure 4b where the switches are controlled by delayed versions of the same unipolar squared pulse $g(t)$. Notice that the unipolar signal that controls the switches is $g(t) = 1$ if $a(t) \geq 0$, and $g(t) = 0$ if $a(t) < 0$. At the output of this SPDT switched feeding network we have the signal $x(t) = k_p p(t) s(t)$, with $s(t)$ being the input signal and $k_p^2 = 1/5$ a normalizing constant resulting from matching the powers of $s(t)$ and $x(t)$ because ideal SPDT switches do not waste power since they have no off-state [18]. For the sake of clarity, the feeding network of Figure 4b (top) is simplified by means of the block diagram labeled "AM" in Figure 4b (bottom) and will be one of the two blocks involved in the synthesis of the dual-beam steerable TMA considered in Section 3.
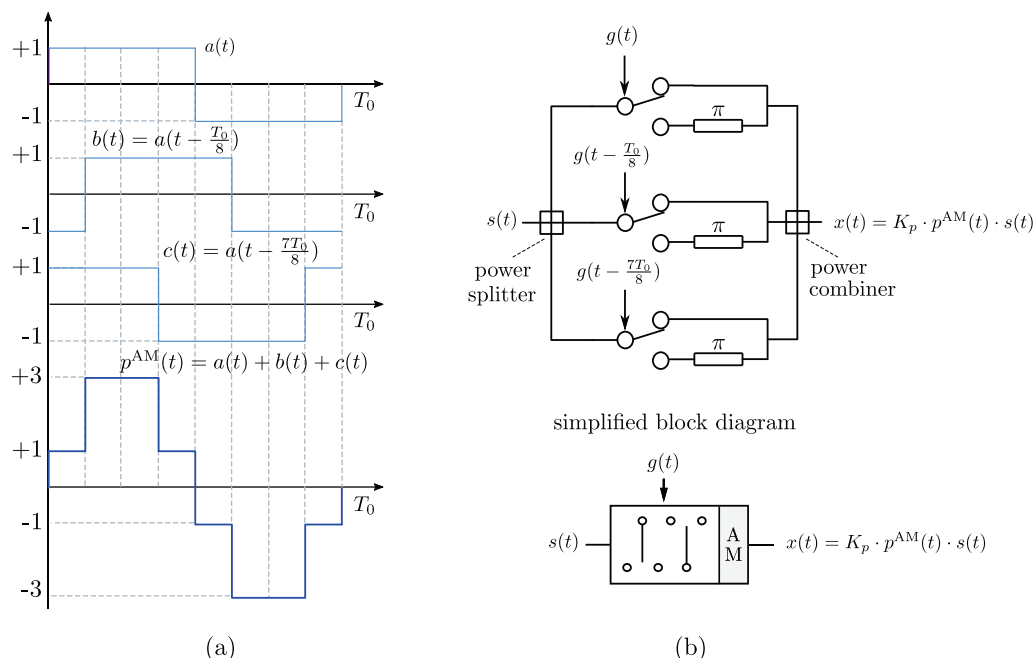
Figure 4. (**a**) Implementation of the periodic AM modulating pulse $p^{\mathrm{AM}}(t)$ from three periodic bipolar square pulses shifted in time. (**b**) SPDT architecture capable of time modulating an input signal $s(t)$ with $p^{\mathrm{AM}}(t)$ (top) and its simplified block diagram (bottom).

The design of a switched network capable of applying the periodical extension of a 4-level linear-phase PM waveform (see Figure 5a) can be realized either with two single-pole four-throw (SP4T) switches (Figure 5b) or with four SPDT switches (Figure 5c). In

both cases, the unipolar signals that control the switches, $h_1(t)$ and $h_2(t)$, and the phase shifts applied to the input signal, $\sphericalangle p^{PM}(t)$, i.e., the phases of $p^{PM}(t)$, are the following:

- $h_1(t) = 0, h_2(t) = 0 \rightarrow \sphericalangle p^{PM}(t) = 0$
- $h_1(t) = 0, h_2(t) = 1 \rightarrow \sphericalangle p^{PM}(t) = \pi/2$
- $h_1(t) = 1, h_2(t) = 0 \rightarrow \sphericalangle p^{PM}(t) = \pi$
- $h_1(t) = 1, h_2(t) = 1 \rightarrow \sphericalangle p^{PM}(t) = 3\pi/2$

Analogously to the AM case, the PM feeding network is abstracted in the block diagram labeled "PM" (see Figure 5d). Notice that for the case of an 8-level linear-phase PM waveform (see Figure 3a) the corresponding switched network can be realized either with two single-pole eight-throw (SP8T) switches or with eight SPDT switches. In both cases, three unipolar control sequences, $h_1(t)$, $h_2(t)$ and $h_3(t)$ will be required.
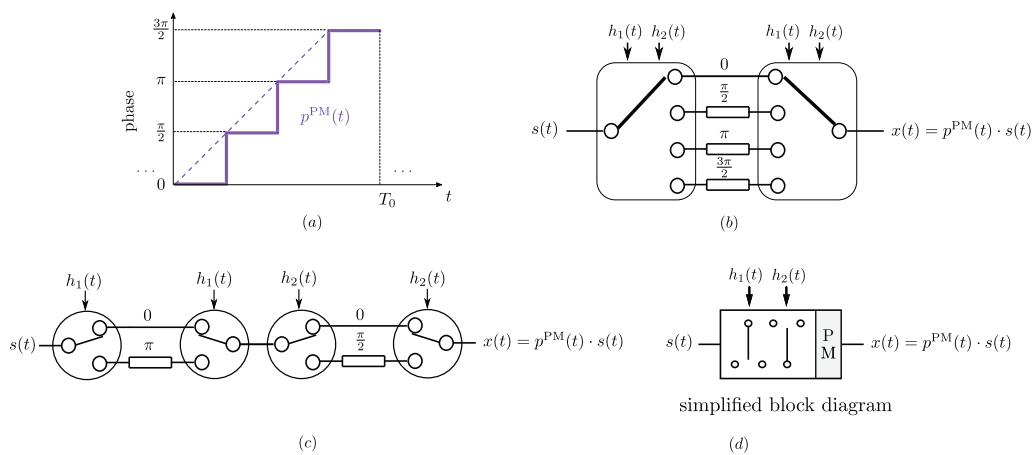
Figure 5. (**a**) 4-level linear phase periodic pulsed waveform $p^{PM}(t)$. (**b**) SP4T architecture capable of time modulating an input signal s(t) with $p^{PM}(t)$. (**c**) SPDT architecture capable of time modulating an input signal s(t) with $p^{PM}(t)$. Note that none of the architectures (**b**,**c**) require power splitters/combiners. (**d**) Equivalent block diagram.

3. Design of Dual-Beam Steerable TMAs Combining AM and PM BFNs

The AM and PM switched modules detailed above are used as the BFN building blocks of a receive dual-beam steerable TMA approach (see a single antenna element in Figure 6). Without loss of generality, in the subsequent analysis we consider the case of a 4-level linear-phase PM switched network. In what follows, we will explain how this feeding network is able to independently steer two antenna array beams by properly selecting the time-delay parameters D_{1n} and D_{2n} shown in Figure 6.
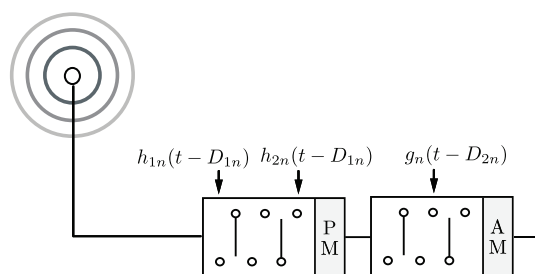
Figure 6. Block diagram of the nth element feeding network of the TMA approach that allows the independent steering of two harmonic beam patterns by combining AM and PM time-modulation.

The array factor (AF) of a TMA (as in any antenna array) represents its response for the case of isotropic elements. The hallmark of the TMA technique is that the array excitations are time-modulated and, as a result, the AF of a TMA is time-variant. Accordingly, by

considering a linear TMA with time modulated excitations $u_n(t)$, $n \in \{0, \ldots N-1\}$, the time-varying AF (explicitly including the term $e^{j\omega_c t}$) is given by

$$F(\theta, t) = e^{j\omega_c t} \sum_{n=0}^{N-1} u_n(t) e^{j\beta_c z_n \cos\theta} \tag{1}$$

where z_n represents the position of the n-th array ideal (i.e., perfectly conductive) isotropic element on the z axis, θ is the angle with respect to such a main axis, and $\beta_c = 2\pi/\lambda_c$ is the wavenumber for a carrier wavelength $\lambda_c = 2\pi c/\omega_c$, being ω_c the carrier frequency.

According to Figure 6, the time modulated excitations are

$$v_n(t) = p^{\mathrm{PM}}(t - D_{1n}) \cdot K_p p^{\mathrm{AM}}(t - D_{2n}) \tag{2}$$

As described below, the time delays D_{1n} and D_{2n} can be selected to accomplish the directions of the main lobes of the two independently-steerable beams (θ_a and θ_b, respectively) in the proposed TMA approach.

By considering the Fourier series expansion of $p^{\mathrm{AM}}(t)$ and $p^{\mathrm{PM}}(t)$ together with the time-shifting property of the Fourier coefficients in Equation (2), we can readily obtain

$$v_n(t) = K_p \sum_{q \in \Psi^{\mathrm{PM}}} P_q^{PM} e^{-jq\omega_0 D_{1n}} e^{jq\omega_0 t} \cdot \sum_{i \in \Psi^{\mathrm{AM}}} P_i^{AM} e^{-ji\omega_0 D_{2n}} e^{ji\omega_0 t} \tag{3}$$

To simplify the notation, we now define the dynamic excitations as

$$_i^q I_n = k_p P_q^{PM} P_i^{AM} e^{-j\omega_0(qD_{1n} + iD_{2n})} \tag{4}$$

Which allows for reducing Equation (3) to

$$v_n(t) = \sum_{q \in \Psi^{\mathrm{PM}}} \sum_{i \in \Psi^{\mathrm{AM}}} {}_i^q I_n e^{j(q+i)\omega_0 t}. \tag{5}$$

Finally, substituting Equation (5) into Equation (1), we arrive at the time-variant AF

$$F(\theta, t) = \sum_{q \in \Psi^{\mathrm{PM}}} \sum_{i \in \Psi^{\mathrm{AM}}} \sum_{n=0}^{N-1} {}_i^q I_n e^{j\beta_c z_n \cos\theta} e^{j(\omega_c + (q+i)\omega_0)t} =$$

$$= \sum_{q \in \Psi^{\mathrm{PM}}} \sum_{i \in \Psi^{\mathrm{AM}}} F_i^q(\theta) e^{j(\omega_c + (q+i)\omega_0)t} \tag{6}$$

where

$$F_i^q(\theta) = \sum_{n=0}^{N-1} {}_i^q I_n e^{j\beta_c z_n \cos\theta} \tag{7}$$

is the spatial AF at the frequency $\omega_c + (q+i)\omega_0$.

In view of Equation (4) and the harmonics profile in Figure 2c,d, we observe that the most meaningful harmonic patterns in Equation (6), in decreasing order of significance, are the ones shown in Table 1. In such a table, we consider the relative level of the maximum of a given harmonic pattern $\left| F_i^q(\theta_{\max}) \right|$ with respect to the maximum of $\left| F_1^1(\theta_{\max}) \right|$ (which we take as a reference pattern) by defining ${}_i^q\Delta_{\mathrm{peak}} = 20\log\left| F_i^q(\theta_{\max})/F_1^1(\theta_{\max}) \right|$, being $\theta_{\max}$ the direction in which an AF amplitude is maximum. According to Table 1, the useful harmonics are $\omega_c + 2\omega_0$ (i.e., $q = i = 1$) and ω_c (i.e., $q = 1$ and $i = -1$) because their beam patterns, $F_{-1}^1(\theta)$ and $F_1^1(\theta)$, have a peak level 9.5 dB above the remaining ones, i.e., the two beam patterns $F_{-1}^1(\theta)$ and $F_1^1(\theta)$ are the ones to be used to perform beam-steering.

Table 1. Characteristics of the dominant harmonic patterns of Equation (6) in decreasing order of significance. Both AM and PM modulating waveforms are 4-level. The useful harmonics are shaded in light blue.

q	i	Frequency	Dynamic Excitations ($_i^q I_n$)	$_i^q \Delta_{\text{Peak}}$ (dB)
1	1	$\omega_c + 2\omega_0$	$k_p P_1^{\text{PM}} P_1^{\text{AM}} \cdot e^{-j\omega_0(D_{1n}+D_{2n})}$	0
1	-1	ω_c	$k_p P_1^{\text{PM}} P_{-1}^{\text{AM}} \cdot e^{-j\omega_0(D_{1n}-D_{2n})}$	0
-3	1	$\omega_c - 2\omega_0$	$k_p P_{-3}^{\text{PM}} P_1^{\text{AM}} \cdot e^{-j\omega_0(-3D_{1n}+D_{2n})}$	-9.5
-3	-1	$\omega_c - 4\omega_0$	$k_p P_{-3}^{\text{PM}} P_{-1}^{\text{AM}} \cdot e^{-j\omega_0(-3D_{1n}-D_{2n})}$	-9.5
1	7	$\omega_c + 8\omega_0$	$k_p P_1^{\text{PM}} P_7^{\text{AM}} \cdot e^{-j\omega_0(D_{1n}+7D_{2n})}$	-16.9
1	-7	$\omega_c - 6\omega_0$	$k_p P_1^{\text{PM}} P_{-7}^{\text{AM}} \cdot e^{-j\omega_0(D_{1n}-7D_{2n})}$	-16.9

We now assume that the array inter-element distance is $\lambda_c/2$. Hence, $\beta_c z_n = \pi n$ and, according to Equation (7) and Equation (4), the spatial AFs of the useful harmonics simplify to

$$F_1^1(\theta) = \sum_{n=0}^{N-1} k_p P_1^{\text{PM}} P_1^{\text{AM}} \cdot e^{j(n\pi\cos\theta - \omega_0(D_{1n}+D_{2n}))},$$

$$F_{-1}^1(\theta) = \sum_{n=0}^{N-1} k_p P_1^{\text{PM}} P_{-1}^{\text{AM}} \cdot e^{j(n\pi\cos\theta - \omega_0(D_{1n}-D_{2n}))} \tag{8}$$

Therefore, if we are willing to steer these beampatterns towards the directions θ_a and θ_b, the following two conditions must, respectively, hold

$$n\pi\cos\theta_a = \omega_0(D_{1n} + D_{2n}),$$

$$n\pi\cos\theta_b = \omega_0(D_{1n} - D_{2n}) \tag{9}$$

which lead to the following time delays

$$D_{1n} = \frac{nT_0(\cos\theta_a + \cos\theta_b)}{4}$$

$$D_{2n} = \frac{nT_0(\cos\theta_a - \cos\theta_b)}{4}. \tag{10}$$

In case of using an 8-level discretization in the PM feeding network, we obtain similar results, but with a higher level of rejection of the undesired harmonics, being the $_i^q\Delta_{\text{peak}}$ values of the most meaningful unwanted harmonics equal to -16.9 dB, as shown in Table 2.

Table 2. Characteristics of the dominant harmonic patterns of Equation (6) in decreasing order of significance for the case of 4-level AM and 8-level PM time-modulating waveforms. The useful harmonics are shaded in light blue.

q	i	Frequency	Dynamic Excitations ($_i^q I_n$)	$_i^q \Delta_{\text{Peak}}$ (dB)
1	1	$\omega_c + 2\omega_0$	$k_p P_1^{\text{PM}} P_1^{\text{AM}} \cdot e^{-j\omega_0(D_{1n}+D_{2n})}$	0
1	-1	ω_c	$k_p P_1^{\text{PM}} P_{-1}^{\text{AM}} \cdot e^{-j\omega_0(D_{1n}-D_{2n})}$	0
1	7	$\omega_c + 8\omega_0$	$k_p P_1^{\text{PM}} P_7^{\text{AM}} \cdot e^{-j\omega_0(D_{1n}+7D_{2n})}$	-16.9
1	-7	$\omega_c - 6\omega_0$	$k_p P_1^{\text{PM}} P_{-7}^{\text{AM}} \cdot e^{-j\omega_0(D_{1n}-7D_{2n})}$	-16.9
-7	1	$\omega_c - 6\omega_0$	$k_p P_{-7}^{\text{PM}} P_1^{\text{AM}} \cdot e^{-j\omega_0(-7D_{1n}+D_{2n})}$	-16.9
-7	-1	$\omega_c - 8\omega_0$	$k_p P_{-7}^{\text{PM}} P_{-1}^{\text{AM}} \cdot e^{-j\omega_0(-7D_{1n}-D_{2n})}$	-16.9

4. Numerical Simulations

An insightful figure of merit to be considered by a TMA designer is the so-called time-modulation radiation efficiency [9] $\eta_{\text{TM}} = \mathcal{P}_U^{\text{TM}}/\mathcal{P}_R^{\text{TM}}$, where $\mathcal{P}_U^{\text{TM}}$ and $\mathcal{P}_R^{\text{TM}}$ are the

useful and total average power values radiated by the TMA, respectively. Notice that η_{TM} accounts for the ability of a TMA to filter out and radiate only over the useful harmonics. By considering $z_n = n\lambda_c/2$ in Equation (1), according to [9,18], we can calculate such an efficiency by means of Equation (4):

$$\eta_{\text{TM}} = \frac{\mathcal{P}_U^{\text{TM}}}{\mathcal{P}_R^{\text{TM}}} = \frac{\sum_{n=0}^{N-1} \left| {}_1^1 I_n \right|^2 + \sum_{n=0}^{N-1} \left| {}_{-1}^1 I_n \right|^2}{\sum_{n=0}^{N-1} \sum_{q \in \Psi^{\text{PM}}} \sum_{i \in \Psi^{\text{AM}}} \left| {}_i^q I_n \right|^2} \tag{11}$$

For the case of a configuration with 4-level AM and 4-level PM waveforms, the radiation efficiency is $\eta_{\text{TM}} = 0.7654$ whereas with 4-level AM and 8-level PM waveforms is $\eta_{\text{TM}} = 0.8974$.

We next consider $f_c = \omega_c/(2\pi) = 2.4\,\text{GHz}$, $f_0 = \omega_0/(2\pi) = 5.5\,\text{MHz}$, $N = 10$ and the four scenarios shown in Figure 7a,b with 4-level AM and 4-level PM modulating waveforms, and (c,d) with 4-level AM and 8-level PM. Different steering directions, θ_a and θ_b, are considered along the scenarios for the exploited harmonics and, accordingly, the normalized time delays D_{1n} and D_{2n} are set after Equation (10). We validate that the dual-beam steerable TMA approach is able to concentrate the radiated power (recall that $\eta_{\text{TM}} = 76.5\%$ and $\eta_{\text{TM}} = 89.8\%$, respectively) on the desired harmonic patterns, $|F_1^1(\theta)|^2$ and $|F_{-1}^1(\theta)|^2$, located at ω_c and $\omega_c + 2\omega_0$, respectively. Hence, simulations show the beam steering and harmonic rejection capabilities of the approach for the two types of discretization of the PM waveform ($-9.5\,\text{dB}$ and $-16.9\,\text{dB}$ respectively). The characteristics of the dominant harmonic patterns are the ones described in Tables 1 and 2 and plotted with a thick line in Figure 7. The limits of the scanning interval that each useful beam pattern is able to support are $33°$ and $147°$. Within these limits the maximum level of undesirable harmonics remain below the threshold indicated in Tables 1 and 2, respectively. The Half Power Beamwidth (HPBW) of the useful harmonics radiation patterns increases slightly as the steering direction separates from the broadside direction.
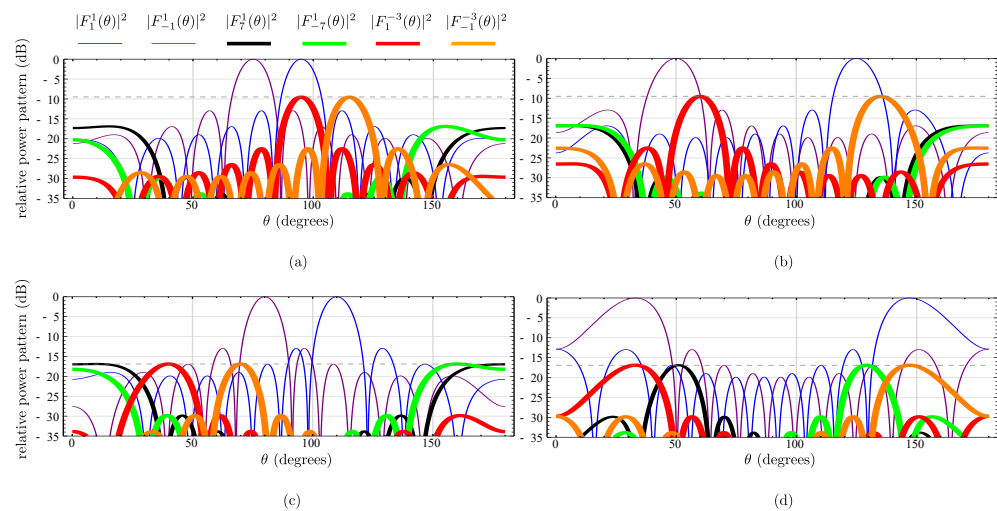
Figure 7. Relative power patterns (dB) for $N = 10$. (**a**) Dual-beam steerable TMA approach in Figure 6, i.e., considering 4-level AM and 4-level PM waveforms where the two useful beam patterns are pointing towards the directions $75°$ and $95°$, respectively. (**b**) The same TMA approach as in (**a**), but the pointing directions are $50°$ and $125°$. (**c**) Dual-beam steerable TMA approach considering 4-level AM and 8-level PM waveforms where the two useful beam patterns are pointing towards the direction of $80°$ and $110°$. (**d**) The same TMA approach as in (**c**), but considering a scenario where the two useful beam patterns point towards $33°$ and $147°$ (i.e., $\pm 57°$ from the broadside direction) which correspond to the limits of the scanning interval that each useful beam pattern is able to support.

5. Comparison with Existing Dual-Beam Architectures

In this section we compare the proposed dual-beam steerable TMA that combines AM and PM switched modulation (Figure 6) with the following equivalent architectures:

(1) standard dual-beam phased arrays employing digital VPS, and (2) dual-beam steerable TMAs capable of offering features similar to the previous ones. To make a fair comparison, existing TMA approaches must be able to do a flexible beamsteering (BS) of the two beams. In the literature about TMAs, the vast majority of papers present a deficient dual-beam capability in the sense that TMAs cannot perform an arbitrary and independent two-beam BS due to the linear dependence between the harmonic excitation phases (see, e.g., [9,13]), thus showing a significant inflexibility. Furthermore, such dual-beam TMAs do not remove the corresponding negative harmonic radiated patterns (or mirrored patterns), i.e., they have no SSB features, being sensibly more inefficient. Hence, within the scope of the existing TMAs, a fair comparison is restricted to dual-beam steerable SSB TMAs [18].

In order to consider the hardware insertion losses in the antenna feeding networks, we must set a suitable framework for comparison. Accordingly, we focus our analysis on the typical WSN band ($f_c = 2.4$ GHz) supporting channels with a bandwidth $B = 5$ MHz. Subsequently, we consider a TMA frequency $f_0 = 5.5$ MHz, and $1/t_{\text{SW}}^{\text{speed}} = 20$ MHz (maximum speed supported by the switches, with $t_{\text{SW}}^{\text{speed}} = t_{\text{ON}} + t_{\text{OFF}} = 50$ ns [18,19]) in order to ensure that the inequality $B < f_0 < 1/t_{\text{SW}}^{\text{speed}}$ [18] is fulfilled. We also select for comparison the less complex version of the proposed design, i.e., the feeding network in Figure 6, in which the corresponding PM block is governed by a 4-level linear phase waveform, and choosing the hardware with SPDT switches shown in Figure 5c.

Table 3 shows the hardware devices considered for the design of the antenna feeding networks in Figure 8. Notice that TMA techniques provide beam steering with an excellent phase sensitivity since the phases of the antenna excitations can be adjusted continuously [7,20] by simply modifying the switch-on time instants of the periodic sequences controlling the switches. Hence, in order to make a fair comparison with standard phase arrays, we consider—as in [18]—high resolution (6 bits) digitally controlled phase shifters [21–23] (see Table 3) leading to phase steps of $\theta_{\text{step}} = 360°/2^6 = 5.6°$. The comparison between the architectures illustrated in Figure 8 focuses on several decisive aspects in WSN: power efficiency, phase sensitivity, complexity, and cost.

Table 3. Examples of devices working in the $f_c = 2.4$ GHz WSN frequency band that can be used in a suitable implementation of the dual-beam steerable arrays in Figure 8.

Device	Frequency (GHz)	Insertion Loss (dB)	References
6-bit VPS	S band	$\eta_{\text{VPS}} = 4.64$	[21–23]
2-way splitter/combiner	1.7–3 (S band)	$\eta_{\text{2-way}} = 0.5$	[24]
3-way splitter/combiner	1.6–2.8 (S band)	$\eta_{\text{3-way}} = 0.8$	[24]
SPDT RF switch	0.05–26.5	$\eta_{\text{SPDT}} = 0.4$	[23]
time delay-line (PCB)	2.4 ± 0.0025	$\eta_{\text{delay-line}} < 0.06$	[25]
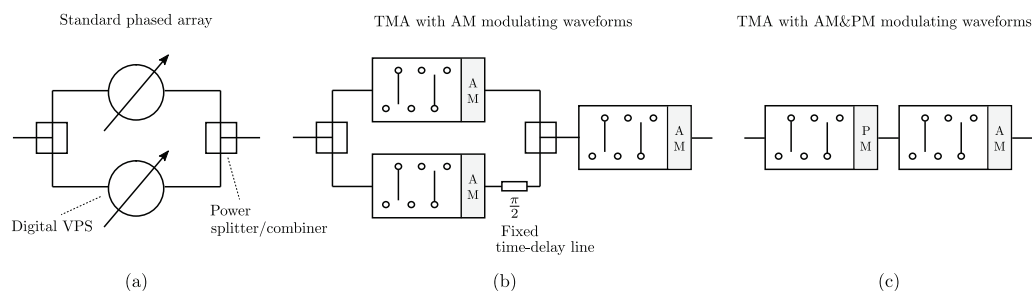
Figure 8. Block diagrams of the corresponding feeding networks of each antenna for different dual-beam steerable array solutions: (**a**) Standard phased array with digital VPSs [26]; (**b**) TMA with AM modulating waveforms [18]; and (**c**) TMA with AM & PM modulating waveforms (this work).

- Power efficiency takes into account the insertion losses associated with the specific hardware devices employed, η_{HW}, and additionally, in the case of the TMA technology, it also considers the time-modulation radiation efficiency, η_{TM} Equation (11), due to the fact that non-useful harmonics are also radiated, hence wasting power.

  In view of Figure 8a, the power efficiency of the dual-beam standard phased array feeding network is

$$\eta_{\mathrm{PA(dB)}} = \eta_{\mathrm{HW(dB)}}^{\mathrm{PA}} = 2\eta_{\text{2-way(dB)}} + \eta_{\mathrm{VPS(dB)}} = 5.64\,\mathrm{dB} \tag{12}$$

  For the case of the TMA architecture in Figure 8b, which was thoroughly analyzed in [18], the power efficiency obeys to

$$\eta_{\mathrm{TMA(dB)}}^{\mathrm{AM}} = \eta_{\mathrm{TM(dB)}}^{\mathrm{AM}} + \eta_{\mathrm{HW(dB)}}^{\mathrm{AM}} \tag{13}$$

  with $\eta_{\mathrm{TM(dB)}}^{\mathrm{AM}} = 0.49$ dB, whereas (see Figure 8b):

$$\eta_{\mathrm{HW(dB)}}^{\mathrm{AM}} = 2\eta_{\mathrm{AM(dB)}}^{\mathrm{module}} + 2\eta_{\text{2-way(dB)}} + \eta_{\text{delay-line(dB)}} \tag{14}$$

  being

$$\eta_{\mathrm{AM(dB)}}^{\mathrm{module}} = 2\eta_{\text{3-way(dB)}} + \eta_{\mathrm{SPDT(dB)}} + \eta_{\text{delay-line(dB)}} \tag{15}$$

  which, by substituting successively the values from Table 3 in Equations (13)–(15), leads to

$$\eta_{\mathrm{TMA(dB)}}^{\mathrm{AM}} = 5.67\,\mathrm{dB} \tag{16}$$

  Regarding the antenna feeding network proposed in this article (see Figure 8c), we have

$$\eta_{\mathrm{HW(dB)}}^{\mathrm{AM/PM}} = \eta_{\mathrm{AM(dB)}}^{\mathrm{module}} + \eta_{\mathrm{PM(dB)}}^{\mathrm{module}} \tag{17}$$

  where

$$\eta_{\mathrm{PM(dB)}}^{\mathrm{module}} = 4\eta_{\mathrm{SPDT(dB)}} + 2\eta_{\text{delay-line(dB)}} \tag{18}$$

  and since $\eta_{\mathrm{TM(dB)}}^{\mathrm{AM/PM}} = -10\log_{10}(0.7654) = 1.16$ dB, we have that (Table 3)

$$\eta_{\mathrm{TMA(dB)}}^{\mathrm{AM/PM}} = \eta_{\mathrm{TM(dB)}}^{\mathrm{AM/PM}} + \eta_{\mathrm{HW(dB)}}^{\mathrm{AM/PM}} = 4.94\,\mathrm{dB} \tag{19}$$

  Note that the proposed antenna feeding network offers the best figure in terms of power efficiency.
- Phase sensitivity. We compare the minimum phase step, θ_{step}, that each steering array architecture is capable of providing. We saw at the beginning of this section that, in the case of a standard phased array (see Figure 8a) with 6-bit VPSs, $\theta_{\mathrm{step}} = 5.6°$. The great advantage of TMA architectures (see Figure 8b,c) is that θ_{step} is directly proportional to $t_{\mathrm{SW}}^{\mathrm{speed}}$ [18]. By considering the SPDT switches in Table 3, with $t_{\mathrm{SW}}^{\mathrm{speed}} = 50$ ns, we achieve (analogously to [18]) a $\theta_{\mathrm{step}} = 1.7°$, which is significantly better than that offered by a standard architecture with 6-bit VPSs.
- The hardware complexity analysis is necessarily centered on two elements: the number of SPDT switches and the number of power splitter/combiners employed by the BFN architecture. Note that a *b*-bit digital phase shifter usually employs 2*b* SPDT switches [21–23]. Thus, the BFN of a standard dual-beam phased array with 6-bit VPSs (see Figure 8a) will have 24 SPDT switches. On the other hand, the dual-beam TMA with AM waveforms shown in Figure 8b requires 9 SPDT switches, whereas the proposed TMA combining AM with PM waveforms (see Figure 8c) uses only 7 SPDT switches. If we now compare the number of power splitter/combiners required by the three architectures, we observe that the TMA architecture with AM waveforms quadruplicates the number of these elements with respect to the other two (i.e., 8 versus 2). Thus, it is concluded that the proposed architecture is objectively the most advantageous in terms of complexity.

- Cost effectiveness. Among all the hardware devices listed in Table 3, the most expensive is clearly the 6-bit VPS. Therefore, we will analyze the percentage of savings of each TMA architecture with respect to the standard phased array. We can see that the strongest differential aspect of the proposed TMA architecture for WSN applications (see Figure 8c) is the significant cost savings. All quantitative results of the comparative are presented in Table 4.

Table 4. Performance comparison –in terms of power efficiency η, phase sensitivity θ_{step}, hardware complexity, and cost effectiveness– between the proposed dual-beam steerable TMA approach controlled with combined AM and PM waveforms (shaded in blue) and competitive solutions existing in the literature.

Architecture	η(dB)	$\theta_{step}(°)$	SPDT Switches	Splitters	TMA Cost Savings (%)
standard PA	5.64	5.6	24	2	-
TMA AM [18]	5.67	1.7	9	8	114.2
TMA AM/PM [this work]	4.94	1.7	7	2	245.2

6. Conclusions and Future Work

An innovative combination of efficient TMA switched feeding networks capable of time-modulating an antenna array with discretized AM and PM waveforms has been proposed. Such architectures are attractive for WSN applications since they allow high resolution dual-beam steering antenna arrays at a reduced complexity and competitive cost.

Although the results of this analysis are promising, we are aware that there are future lines of research that remain open. Next steps are the realization of full-wave simulations, and the construction and characterization of a hardware prototype.

Author Contributions: R.M.-C. participated in the tasks: conceptualization, formal analysis, research, software, visualization and writing—original draft. J.B. participated in the tasks: conceptualization, research, and writing—review & editing. J.A.G.-N. participated in the tasks: funding acquisition, visualization, project administration and writing—review & editing. L.C. participated in the tasks: visualization, project administration and writing—review & editing. All authors have read and agreed to the published version of the manuscript.

Institutional Review Board Statement: Not applicable.

Informed Consent Statement: Not applicable.

Data Availability Statement: Not applicable.

Conflicts of Interest: The authors declare no conflict of interest. The funders had no role in the design of the study; in the collection, analyses, or interpretation of data; in the writing of the manuscript, or in the decision to publish the results.

Abbreviations

The following abbreviations are used in this manuscript:

AF	array factor
AM	amplitude modulation
BS	beamsteering
BFN	beamforming network
DOA	direction of arrival
DSB	double sideband
PM	phase modulation
RF	radio frequency
SP4T	single-pole four-throw
SP8T	single-pole eight-throw
SPDT	single-pole dual-throw
SSB	single sideband
TMA	time-modulated array
VPS	variable phase shifter
ULA	uniform linear array
WSN	wireless sensor network

References

1. Senouci, M.R.; Mellouk, A. *Deploying Wireless Sensor Networks: Theory and Practice*; ISTE Press-Elsevier: London, UK, 2016.
2. Curiac, D.I. Wireless Sensor Network Security Enhancement Using Directional Antennas: State of the Art and Research Challenges. *Sensors* **2016**, *16*, 488. [CrossRef] [PubMed]
3. George, R.; Mary, T.A.J. Review on directional antenna for wireless sensor network applications. *IET Commun.* **2020**, *14*, 715–722. [CrossRef]
4. Mottola, L.; Voigt, T.; Picco, G.P. Electronically-switched directional antennas for wireless sensor networks: A full-stack evaluation. In Proceedings of the 2013 IEEE International Conference on Sensing, Communications and Networking (SECON), New Orleans, LA, USA, 24–27 June 2013; pp. 176–184. [CrossRef]
5. Catarinucci, L.; Guglielmi, S.; Colella, R.; Tarricone, L. Switched-beam antenna for WSN nodes enabling hardware-driven power saving. In Proceedings of the 2014 Federated Conference on Computer Science and Information Systems, Warsaw, Poland, 7–10 September 2014; pp. 1079–1086. [CrossRef]
6. Maneiro-Catoira, R.; Brégains, J.; García-Naya, J.A.; Castedo, L. Time Modulated Arrays: From their Origin to their Utilization in Wireless Communication Systems. *Sensors* **2017**, *17*, 590. [CrossRef] [PubMed]
7. Chen, Q.; Zhang, J.; Wu, W.; Fang, D. Enhanced Single-Sideband Time-Modulated Phased Array with Lower Sideband Level and Loss. *IEEE Trans. Antennas Propag.* **2020**, *68*, 275–286. [CrossRef]
8. Chen, Q.; Bai, L.; He, C.; Jin, R. On the Harmonic Selection and Performance Verification in Time-Modulated Array-Based Space Division Multiple Access. *IEEE Trans. Antennas Propag.* **2021**, *69*, 3244–3256. [CrossRef]
9. Maneiro Catoira, R.; Brégains, J.; Garcia-Naya, J.A.; Castedo, L.; Rocca, P.; Poli, L. Performance Analysis of Time-Modulated Arrays for the Angle Diversity Reception of Digital Linear Modulated Signals. *IEEE J. Sel. Top. Signal Process.* **2017**, *11*, 247–258. [CrossRef]
10. Li, G.; Yang, S.; Nie, Z. Direction of Arrival Estimation in Time Modulated Linear Arrays With Unidirectional Phase Center Motion. *IEEE Trans. Antennas Propag.* **2010**, *58*, 1105–1111. [CrossRef]
11. He, C.; Cao, A.; Chen, J.; Liang, X.; Zhu, W.; Geng, J.; Jin, R. Direction Finding by Time-Modulated Linear Array. *IEEE Trans. Antennas Propag.* **2018**, *66*, 3642–3652. [CrossRef]
12. He, C.; Liang, X.; Li, Z.; Geng, J.; Jin, R. Direction Finding by Time-Modulated Array With Harmonic Characteristic Analysis. *IEEE Antennas Wirel. Propag. Lett.* **2015**, *14*, 642–645. [CrossRef]
13. Rocca, P.; Zhu, Q.; Bekele, E.; Yang, S.; Massa, A. 4-D Arrays as Enabling Technology for Cognitive Radio Systems. *IEEE Trans. Antennas Propag.* **2014**, *62*, 1102–1116. [CrossRef]
14. Zhu, Q.; Yang, S.; Yao, R.; Nie, Z. Directional Modulation Based on 4-D Antenna Arrays. *IEEE Trans. Antennas Propag.* **2014**, *62*, 621–628. [CrossRef]
15. Bogdan, G.; Yashchyshyn, Y.; Jarzynka, M. Time-Modulated Antenna Array With Lossless Switching Network. *IEEE Antennas Wirel. Propag. Lett.* **2016**, *15*, 1827–1830. [CrossRef]
16. Yao, A.M.; Wu, W.; Fang, D.G. Single-Sideband Time-Modulated Phased Array. *IEEE Trans. Antennas Propag.* **2015**, *63*, 1957–1968. [CrossRef]
17. Bogdan, G.; Godziszewski, K.; Yashchyshyn, Y.; Kim, C.H.; Hyun, S. Time Modulated Antenna Array for Real-Time Adaptation in Wideband Wireless Systems-Part I: Design and Characterization. *IEEE Trans. Antennas Propag.* **2019**, *68*, 6964–6972. [CrossRef]
18. Maneiro-Catoira, R.; García-Naya, J.A.; Brégains, J.C.; Castedo, L. Multibeam Single-Sideband Time-Modulated Arrays. *IEEE Access* **2020**, *8*, 151976–151989. [CrossRef]

19. Understanding RF/Microwave Solid State Switches and Their Applications. Keysight Application Note. Available online: http://www.keysight.com/us/en/assets/7018-01705/application-notes/5989-7618.pdf (accessed on 1 January 2022).
20. Zeng, Q.; Yang, P.; Yin, L.; Lin, H.; Wu, C.; Yang, F.; Yang, S. Phase Modulation Technique for Harmonic Beamforming in Time-Modulated Arrays. *IEEE Trans. Antennas Propag.* 2021, *in press*. [CrossRef]
21. Analog Devices. SPDT Switches, DVariable Phase Shifters. HMC545A. HMC649A, HMC642A. Available online: https://www.analog.com (accessed on 1 January 2022).
22. Qorvo. Monolithic Microwave Integrated Circuit (MMIC) Digital Phase Shifters. Available online: http://www.qorvo.com (accessed on 1 January 2022).
23. Macom. MMIC Digital Phase Shifters and SPMT Switches: MASW-00x100 Series. Available online: https://www.macom.com (accessed on 1 January 2022).
24. Minicircuits. Available online: http://www.minicircuits.com (accessed on 1 January 2022).
25. Rogers. RO4000 Hydrocarbon Ceramic Laminates. Available online: https://www.rogerscorp.com (accessed on 1 January 2022).
26. Hong, W.; Jiang, Z.H.; Yu, C.; Zhou, J.; Chen, P.; Yu, Z.; Zhang, H.; Yang, B.; Pang, X.; Jiang, M.; et al. Multibeam Antenna Technologies for 5G Wireless Communications. *IEEE Trans. Antennas Propag.* **2017**, *65*, 6231–6249. [CrossRef]